Cancer Cell
Article

Reduced H3K27me3 and DNA Hypomethylation Are Major Drivers of Gene Expression in K27M Mutant Pediatric High-Grade Gliomas

Sebastian Bender,[1,2,23] Yujie Tang,[3,4,23] Anders M. Lindroth,[5,23] Volker Hovestadt,[6] David T.W. Jones,[1] Marcel Kool,[1] Marc Zapatka,[6] Paul A. Northcott,[1] Dominik Sturm,[1] Wei Wang,[6] Bernhard Radlwimmer,[6] Jonas W. Højfeldt,[7] Nathalène Truffaux,[8] David Castel,[8] Simone Schubert,[3,4] Marina Ryzhova,[9] Huriye Şeker-Cin,[1] Jan Gronych,[6] Pascal David Johann,[1,2] Sebastian Stark,[1,10] Jochen Meyer,[11,12] Till Milde,[13,14] Martin Schuhmann,[15] Martin Ebinger,[16] Camelia-Maria Monoranu,[17] Anitha Ponnuswami,[3] Spenser Chen,[3] Chris Jones,[18] Olaf Witt,[13,14] V. Peter Collins,[19] Andreas von Deimling,[11,12] Nada Jabado,[20] Stephanie Puget,[21] Jacques Grill,[8] Kristian Helin,[7] Andrey Korshunov,[11,12] Peter Lichter,[6] Michelle Monje,[3,4,22] Christoph Plass,[5,24,*] Yoon-Jae Cho,[3,4,24,*] and Stefan M. Pfister[1,2,24,*]

[1]Division of Pediatric Neurooncology, German Cancer Research Center (DKFZ), 69120 Heidelberg, Germany
[2]Department of Pediatric Oncology, Hematology, and Immunology, Heidelberg University Hospital, 69120 Heidelberg, Germany
[3]Department of Neurology and Neurological Sciences, Stanford University School of Medicine, Stanford, CA 94305, USA
[4]Department of Neurosurgery, Stanford University School of Medicine, Stanford, CA 94305, USA
[5]Division of Epigenomics and Cancer Risk Factors, German Cancer Research Center (DKFZ), 69120 Heidelberg, Germany
[6]Division of Molecular Genetics, German Cancer Research Center (DKFZ), 69120 Heidelberg, Germany
[7]Biotech Research and Innovation Centre (BRIC) and Centre for Epigenetics, University of Copenhagen, 2200 Copenhagen, Denmark
[8]Institut Gustave Roussy, Laboratoire de Vectorologie et Thérapeutiques Anticancéreuses, Unité Miste de Recherche du Centre National de la Recherche Scientifique (CNRS) 8203, Université Paris Sud, Villejuif 94800, France
[9]Department of Neuropathology, NN Burdenko Neurosurgical Institute, Moscow 125047, Russia
[10]Department of General Pediatrics, Heidelberg University Hospital, 69120 Heidelberg, Germany
[11]Department of Neuropathology, Heidelberg University Hospital, 69120 Heidelberg, Germany
[12]Clinical Cooperation Unit Neuropathology, German Cancer Research Center (DKFZ), 69120 Heidelberg, Germany
[13]Clinical Cooperation Unit Pediatric Oncology, German Cancer Research Center (DKFZ), 69120 Heidelberg, Germany
[14]Section of Pediatric Brain Tumors, Department of Pediatric Oncology, Hematology and Immunology, Heidelberg University Hospital, 69120 Heidelberg, Germany
[15]Department of Neurosurgery, University Hospital Tübingen, 72076 Tübingen, Germany
[16]Department of Hematology and Oncology, Children's University Hospital Tübingen, 72076 Tübingen, Germany
[17]Department of Neuropathology, Institute of Pathology, University Würzburg, 97080 Würzburg, Germany
[18]Divisions of Molecular Pathology and Cancer Therapeutics, The Institute of Cancer Research, Sutton, Surrey 5NG, UK
[19]Division of Molecular Histopathology, Department of Pathology, University of Cambridge, Cambridge 0QQ, UK
[20]Departments of Pediatrics and Human Genetics, McGill University and the McGill University Health Center Research Institute, Montreal, QC H3Z 2Z3, Canada
[21]Département de Neurochirurgie Pédiatrique et Unité 845, l'Institut National Recherche Médicale (INSERM), Université Paris V Descartes, Hôpital Necker Enfants Malades, 75743 Paris, France
[22]Department of Pediatrics, Stanford University School of Medicine, Stanford, CA 94305, USA
[23]These authors contributed equally to this work
[24]Co-senior authors
*Correspondence: c.plass@dkfz.de (C.P.), yjcho1@stanford.edu (Y.-J.C.), s.pfister@dkfz.de (S.M.P.)
http://dx.doi.org/10.1016/j.ccr.2013.10.006

SUMMARY

Two recurrent mutations, K27M and G34R/V, within histone variant H3.3 were recently identified in ~50% of pHGGs. Both mutations define clinically and biologically distinct subgroups of pHGGs. Here, we provide further insight about the dominant-negative effect of K27M mutant H3.3, leading to a global reduction of

Significance

Loss of polycomb repression, which is reflected by reduced H3K27me3 levels, is associated with unfavorable prognosis in several cancer entities. Here, we highlight the molecular mechanism of global H3K27me3 loss in pHGGs harboring the K27M mutation of histone H3.3. Additionally, we provide evidence that H3K27me3 occupancy as well as DNA methylation are specifically altered in K27M mutant pHGGs. Both deregulated epigenetic mechanisms cooperate to establish a transcriptional program that is specific for K27M mutant pHGGs. In conclusion, our data shed light on the molecular consequences induced by one of the two histone H3.3 mutations driving tumorigenesis in ~50% of pHGGs.

the repressive histone mark H3K27me3. We demonstrate that this is caused by aberrant recruitment of the PRC2 complex to K27M mutant H3.3 and enzymatic inhibition of the H3K27me3-establishing methyltransferase EZH2. By performing chromatin immunoprecipitation followed by next-generation sequencing and whole-genome bisulfite sequencing in primary pHGGs, we show that reduced H3K27me3 levels and DNA hypomethylation act in concert to activate gene expression in K27M mutant pHGGs.

INTRODUCTION

Pediatric high-grade gliomas (pHGGs), which include glioblastomas and diffuse intrinsic pontine gliomas (DIPGs), represent a highly malignant type of brain tumor in children, which is reflected by a 3-year overall survival rate of only 5%–10% (Louis et al., 2007). Similar to other cancers, comprehensive sequencing studies have revealed a variety of genetic abnormalities in chromatin remodeling factors in pHGGs (Fontebasso et al., 2013). However, unique to HGGs in children and adolescents are two recurrent mutations within the histone H3.3 gene *H3F3A*, which have been identified in ~50% of cases (Schwartzentruber et al., 2012; Wu et al., 2012). These two mutations result in substitutions at residues K27 and G34 on the amino-terminal tail of H3.3. The K27 mutations universally substitute the K27 with a methionine (K27M), whereas the G34 mutations typically replace the G34 with an arginine (G34R), and in some cases with a valine (G34V). Similar mutations have also been reported at a lower frequency in *HIST1H3B*, which encodes the canonical histone H3.1. These *HIST1H3B* mutations have exclusively been identified in DIPGs (Wu et al., 2012). Interestingly, K27M and G34R/V mutations are associated not only with clinical parameters such as patient age or tumor location, but they also exhibit a mutation-specific gene expression and DNA methylation profile (Khuong-Quang et al., 2012; Sturm et al., 2012). Recently, it has been reported that K27M mutant pHGGs display a global decrease of the repressive posttranslational histone modification H3K27me3 (Chan et al., 2013; Lewis et al., 2013; Venneti et al., 2013), which under physiological conditions is mainly established by the H3K27-specific histone methyltransferase enhancer of zeste 2 (EZH2) within the Polycomb Repressive Complex 2 (PRC2) (Margueron and Reinberg, 2011). Mechanistically, reduction of H3K27me3 levels is caused by an inhibitory effect of the K27M mutant H3.3 protein (Lewis et al., 2013).

In this study, we explore the dominant-negative effect of K27M mutant H3.3 and the association of K27M-induced H3K27me3 reduction with DNA methylation and gene expression.

RESULTS

H3K27me3 Is Strongly Reduced in K27M Mutant pHGGs

Recent studies have reported a reduction of H3K27me3 levels in K27M mutant pHGGs by using immunohistochemistry (IHC) on small numbers of patient samples ($n \leq 20$ tumors; Lewis et al., 2013; Venneti et al., 2013). To investigate whether immunohistochemical testing of H3K27me3 abundance in pHGGs might be useful for routine clinical application, we performed IHC for H3K27me3 in a large cohort of pHGGs with known *H3F3A* mutation status (n = 104). Strikingly, all K27M mutant pHGGs (n = 21) showed a strong reduction of overall H3K27me3 levels (Figure 1A), even though the antibody detects H3K27me3 at all H3 variants including canonical histone proteins. H3K27me3-positive endothelial cells lining the blood vessels show that H3K27me3 is specifically lost in the tumor cells (Figure 1B). In contrast, all G34R/V mutant cases (n = 7) and 74 out of 76 pHGGs (97%) without H3.3 mutation (wild-type H3.3 [H3.3-WT]) were strongly positive for H3K27me3. No mutation of canonical H3.1 was found in the two H3K27me3-negative tumors without H3.3 mutation. The average number of H3K27me3 immunopositive cell nuclei in K27M mutant pHGGs did not exceed 8% (average, 5%) compared with at least 71% (average, 95%) of H3K27me3-positive cell nuclei in non-K27M tumor cores (Figure 1C). Moreover, no global differences were observed for several other key histone marks including H3K4me3, H3K9me3, and H3K36me3, which are all known to also substantially influence chromatin structure and gene expression. Immunopositivity for these three histone marks was detected in all analyzed tumor samples (data not shown).

To further confirm the IHC results, we isolated histone extracts from a non-overlapping cohort of additional primary pHGG samples and studied H3K27me3 levels by western blot analysis. Two different H3K27me3-specific antibodies detected significantly lower H3K27me3 levels in all K27M mutant tumors (n = 3) compared with H3.3-WT samples (n = 2) and a G34R mutant tumor (Figure 1D).

We also determined H3K27me3 levels in a set of primary cultures/cell lines, which cover the whole spectrum of H3.3 mutations that have been identified in primary pHGG tumors. We used primary cell lines established from freshly resected K27M mutant pHGGs (NEM157 and NEM165) as well as a G34R mutant tumor (MGBM1) and compared them with the levels in a human embryonal kidney cell line (HEK293T, H3.3-WT), human epithelial carcinoma cells (HeLa-S3, H3.3-WT), and two well-established pediatric glioblastoma cell lines (SF188, H3.3-WT and KNS42, H3.3-G34V). Whereas H3K27me3 levels were found to be subject to fluctuations in non-K27M cell types (very high in HEK293T, low in MGBM1), H3K27me3 was almost completely absent in NEM157 and NEM165 cells, which harbor a heterozygous K27M mutation (Figure 1E).

H3.3-K27M Is a Dominant-Negative Inhibitor of H3K27 Di- and Trimethylation

All described *H3F3A* mutations in primary tumors and cell lines are heterozygous and thus affect only one *H3F3A* allele, indicating a dominant-negative effect of the K27M mutant protein on the wild-type histone H3 protein. Although transgene-induced reduction of H3K27me3 was shown to take place in a cell-type-independent manner in HEK293T, human astrocytes, mouse embryonic fibroblasts, and human neural stem cells (NSCs; Chan et al., 2013; Lewis et al., 2013), we aimed to mimic the genetic background of pHGGs more closely by generating isogenic SF188 glioblastoma cells stably overexpressing ectopic

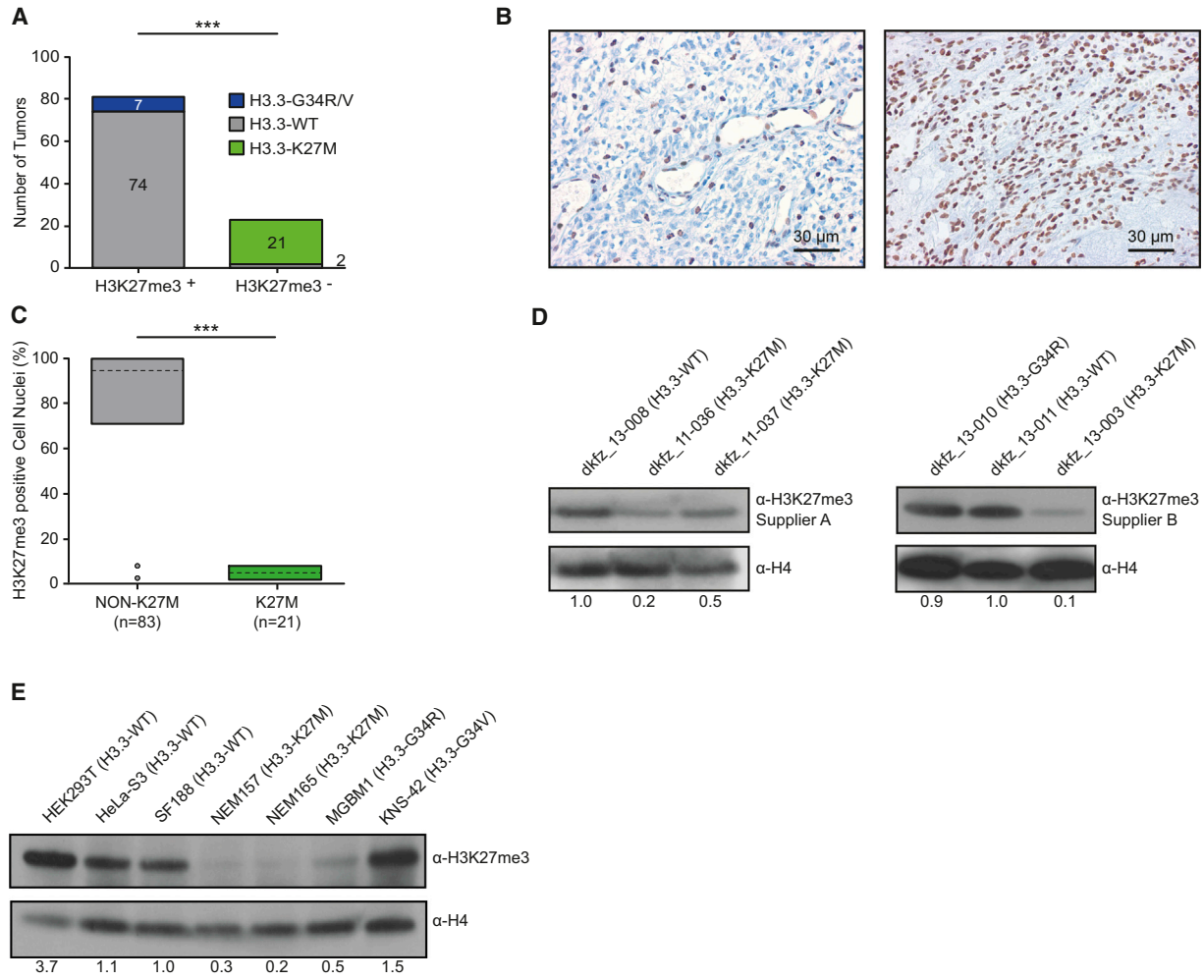

Figure 1. pHGGs Carrying Histone H3.3-K27M Mutations Show a Global Reduction of K27 Trimethylation on Histone H3

(A) Summary of H3K27me3 immunostaining of 104 pHGGs containing wild-type (H3.3-WT), K27M mutant, or G34R/V mutant H3.3 (***$p < 0.001$).

(B) Representative results of immunohistochemistry for H3K27me3 of a K27M mutant (left) and H3.3-WT (right) pHGG.

(C) Quantification of H3K27me3 positive cell nuclei in pHGGs without (non-K27M) or with the K27M mutation (200 cell nuclei/tumor) (***$p < 0.001$). Box plots represent the maximum/minimum number (%) of H3K27me3 positive cell nuclei. The mean is indicated by the dashed line.

(D) Western blot analysis of histone extracts from primary pHGGs using two different H3K27me3-specific antibodies. Numbers below the western blots indicate H3K27me3 band intensity (normalized to total histone H4) measured by using ImageJ.

(E) Evaluation of H3K27me3 expression in patient-derived pHGG cell lines, HEK293T, and HeLa-S3 cells. Numbers below the western blots indicate H3K27me3 band intensity (normalized to total histone H4) measured by using ImageJ.

wild-type, K27M or G34R mutant H3.3. Initially, at 6 days after transduction, K27M-expressing SF188 cells did not show differences in H3K27 trimethylation compared with cells overexpressing H3.3-WT or the G34R variant (Figure S1A available online). However, it was previously reported that reshaping of the epigenome occurs over an extended time period (Turcan et al., 2012). In line with this, Chan et al. (2013) showed that K27M-induced reduction of H3K27me3 is dependent on several cell divisions. Therefore, we re-analyzed transduced SF188 cells maintained in culture for 70 days (25 passages). At this later time point, H3K27me3 levels were significantly reduced in SF188 cells expressing the K27M mutant (Figure 2A). We further verified this regulatory effect of the K27M transgene on global H3K27me3 levels in vitro by using wild-type, K27M-transduced, or G34R-transduced HEK293T, cultured for the same time period (Figure 2A).

To confirm the dominant-negative effect of the K27M mutant on endogenous H3 histones, we immunoprecipitated mononucleosomes using epitope-tagged wild-type or K27M mutant H3.3 expressed in SF188, HEK293T, and HeLa-S3 cells for at least 10 days. As expected, mono-, di-, and trimethylation of H3K27 was absent on exogenous K27M mutant H3.3 (Figure 2B, labeled with *). In addition, reduced di- and trimethylation was also detected at endogenous wild-type H3 proteins within the same nucleosomes (Figure 2B, labeled with **; Table S1) as well as with global endogenous H3 protein (Figure 2B, labeled with ***; Table S1). Notably, H3K27me1 levels were found to be unchanged at wild-type H3 within the same nucleosome, as

well as overall endogenous H3 protein (Figure 2B). Together, our results strongly suggest that K27M mutant H3.3 interferes with PRC2 function, as this complex is responsible for di- and trimethylation (but not monomethylation) of H3K27 through its enzymatic subunit EZH2 (Margueron and Reinberg, 2011).

K27M Mutant H3.3 Aberrantly Binds PRC2 and Interferes with Its Enzymatic Activity

Di- and trimethylation of K27 at histone H3 is mainly mediated by the nonredundant H3K27-specific histone methyltransferase EZH2, which is part of PRC2. Recently, it has been reported that synthetic peptides containing the K27M mutant interact with the catalytic site of EZH2 (Lewis et al., 2013). By performing coimmunoprecipitation (coIP) experiments in SF188, HEK293T, and HeLa-S3 cells ectopically expressing HA-tagged wild-type or K27M mutant H3.3, we found that EZH2 as well as the PRC2 component suppressor of zeste homolog 12 (SUZ12) was dramatically enriched in immunoprecipitated K27M-containing mono-nucleosomes relative to wild-type H3.3 protein in all three cell lines (Figure 2C; Table S1). Conversely, coIP for endogenous EZH2 in all three cell lines led to an enrichment of exogenous K27M mutant H3.3 compared with the exogenous wild-type H3.3 protein (Figure 2D).

Next, we investigated whether PRC2 complexes bound to K27M mutant H3.3 were associated with an altered enzymatic activity of EZH2. Using total chromatin lysate and an immunoprecipitation (IP) fraction bound to anti-HA beads from both wild-type H3.3 and K27M-transduced SF188, HEK293T, or HeLa-S3 cells, we performed in vitro histone methyltransferase (HMT) assays. We observed a significant decrease of HMT activity of 40%–70% with chromatin lysate from all three K27M-transduced cell lines. Even more strikingly, with the IP fraction composed of K27M-containing mono-nucleosomes from each cell line, EZH2 enzymatic activity was decreased by at least 85% (Figure 2E; Figure S1B). To evaluate the inhibitory effect of K27M mutant H3.3 on EZH2 catalytic activity, we determined the IC_{50} value of K27M-containing peptides and compared it with the highly potent and selective small molecule EZH2-inhibitor GSK343 (Verma et al., 2012). Whereas addition of wild-type H3.3 peptide was found to have a stimulatory effect on PRC2 activity (Figure S1C), the IC_{50} value of the K27M-containing peptide (0.067 μM) was in a range similar to that of GSK343 (0.027 μM) (Figure 2F). Instead of using synthetic peptides, we also performed in vitro HMT assays using oligonucleosomes purified directly from K27M mutant NEM157 cells or SF188 cells (H3.3-WT). The addition of oligonucleosomes purified from NEM157 cells led to a significant inhibition of PRC2 enzymatic activity compared with SF188 oligonucleosomes (Figure S1D).

In contrast, the enzymatic activities of the H3K27me3 demethylases JMJD3/UTX were found to remain largely unchanged between wild-type and K27M-containing mono-nucleosomes when tested with the same chromatin lysates and IP-bound fractions (Figure 2G).

Genome-wide Analysis of H3K27me3 in K27M Mutant pHGGs

To generate genome-wide maps of H3K27me3 in primary K27M mutant pHGGs, we performed chromatin IP followed by next-generation sequencing (ChIP-Seq) on fresh-frozen primary tumor tissue from two K27M mutant pHGGs and two pHGGs without H3.3 mutation. In addition, we conducted H3K27me3 ChIP-Seq in the K27M mutant primary cell line NEM165 as well as the established pediatric glioblastoma cell line SF188 (H3.3-WT). As expected, the identified number of H3K27me3 ChIP-Seq peaks in both K27M mutant pHGGs was substantially lower across the entire genome (promoter: transcriptional start site [TSS] ± 3 kb, gene body, intergenic regions) compared with both H3.3-WT tumors (Figure 3A). The proportions of overlapping ChIP-Seq peaks among H3.3-WT pHGGs and among K27M mutant tumors were comparable (37% overlapping H3K27me3 peaks in both groups; Figure 3B). In line with the K27M-induced reduction of H3K27me3, the number of H3K27me3 peaks unique to H3.3-WT tumors was four times of the number of peaks unique to K27M mutant pHGGs (Figure 3B).

Although global H3K27me3 levels detected by western blot are dramatically reduced in K27M mutant NEM165 cells (Figure 1E), there was no clear reduction in peak number in these cells compared with SF188 cells (Figure 3A). Moreover, only 57% of ChIP-Seq Peaks detected in NEM165 cells overlapped with peaks detected in at least one of the K27M mutant primary tumors (Figure 3B). In contrast, we identified a higher concordance between SF188 cells and H3.3-WT primary tumors (92% overlapping ChIP-Seq peaks).

Next, we looked at global differences in H3K27me3 ChIP-Seq peaks (n = 21,217) identified in primary tumors (Figure 4A). In total, 75% of all detected H3K27me3 peaks were found to be reduced or lost in K27M mutant tumors (n = 15,853). However, our analysis also revealed a significant number of H3K27me3 peaks showing increased H3K27me3 occupancy in K27M mutant tumors (n = 5,364). Even more interestingly, peaks with reduced H3K27me3 levels had a significantly different genomic location to peaks with increased H3K27me3 occupancy (χ^2 test; $p < 0.01$). Peaks with reduced and increased H3K27me3 levels in K27M mutant tumors were more frequently associated with gene promoters and intergenic regions, respectively (Figure 4A).

In order to find out to what extent our in vitro cultures recapitulate H3K27me3 occupancy in primary pHGGs, we conducted a similar analysis with global peak distribution for the analyzed cell lines (NEM165 and SF188). This highlighted substantial differences in H3K27me3 distribution between primary tumors and both cell lines (Figures S2A and S2B). Due to these differences, ChIP-Seq data from in vitro cultures were excluded from subsequent analyses.

Alterations in H3K27me3 occupancy in the promoter have been shown to affect gene expression. Therefore, we compared gene expression data of 12 K27M mutant tumors and 10 pHGGs without H3.3 mutations to specifically analyze H3K27me3 occupancy around the TSS of differentially expressed genes. In doing so, we identified a total of 294 genes as being differentially expressed ($p < 0.01$; Student's t test, Benjamini-Hochberg correction; Figure S2C; Table S2). Gene ontology analysis of differentially expressed genes revealed a significant enrichment of genes involved in neuronal differentiation (Table S3). Compared with all other genes, differentially expressed genes were found to be significantly overrepresented within our set of genes showing alterations in H3K27me3 ($p < 0.01$, Fisher's exact test). Remarkably, 66% (95 out of 143) of transcriptionally

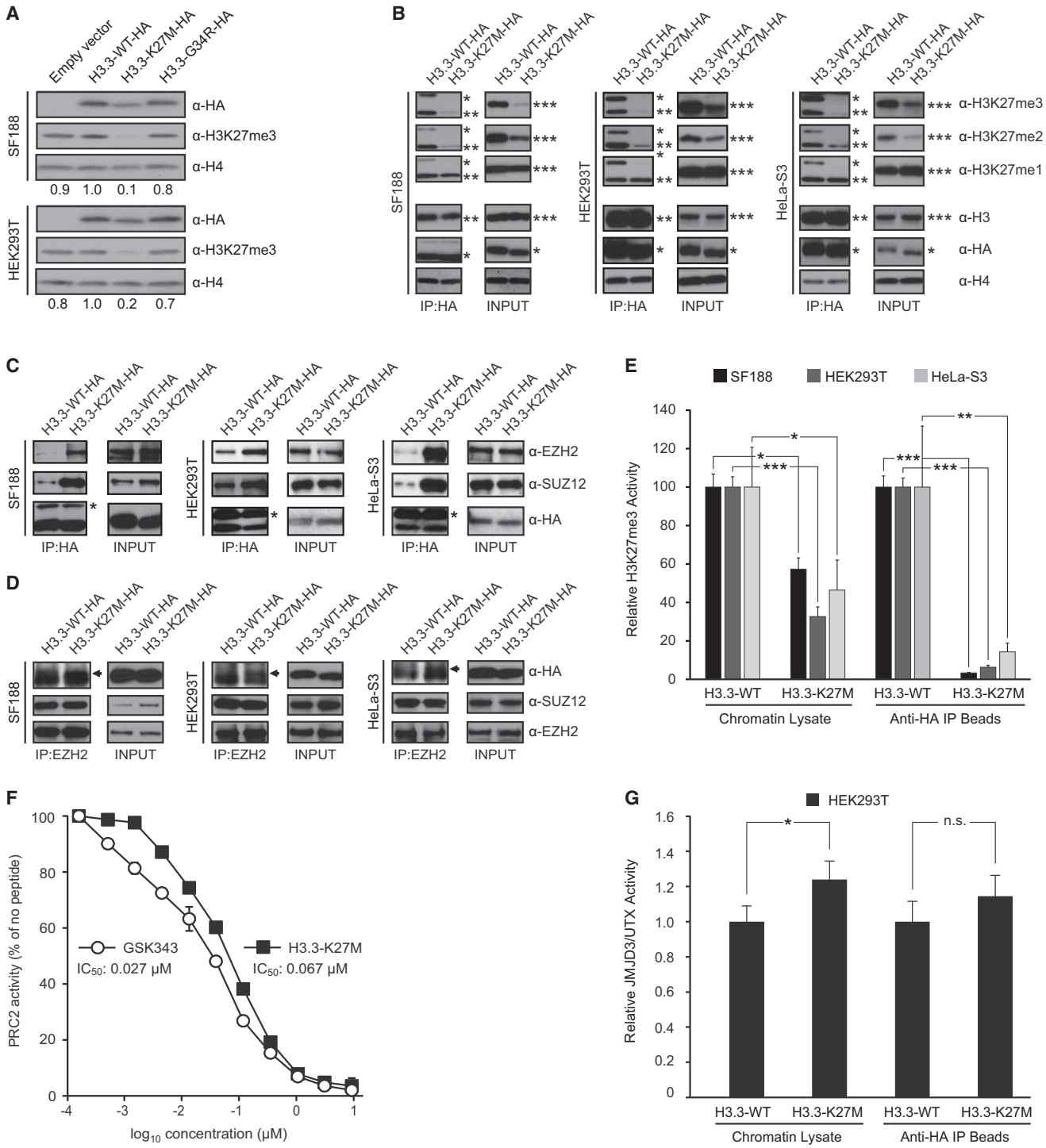

Figure 2. K27M Mutant H3.3 Exerts a Dominant-Negative Effect on the Methylation State of Wild-Type H3K27

(A) Western blot of H3K27me3 in histone extracts from SF188 and HEK293T cells transduced with HA-tagged H3.3 (WT, K27M, or G34R). Numbers below the western blot indicate H3K27me3 band intensity (normalized to total histone H4) measured by using ImageJ.

(B) Western blot analysis of methylated marks on mono-nucleosome immunoprecipitates of HA-tagged histone H3.3 in SF188, HEK293T, and HeLa-S3 cells. The symbols * and ** denote exogenous HA-tagged histone H3.3 and endogenous histone H3 within mono-nucleosomes, respectively; *** denotes total endogenous histone H3. Anti-histone H3, H4, anti-HA, and input protein lysates are shown as controls.

(C) Western blot analysis of EZH2 and SUZ12 in immunorecipitates of exogenous HA-tagged histone H3.3 (WT or K27M) expressed in SF188, HEK293T, or HeLa-S3 cells. Anti-HA is shown as loading control. The * denotes IgG light chain.

(D) Exogenous HA-tagged H3.3 (WT or K27M) coimmunoprecipitated with endogenous EZH2 in SF188, HEK293T, and HeLa-S3 cells was detected by western blot analysis. Anti-EZH2 and anti-SUZ12 are shown as loading controls.

(legend continued on next page)

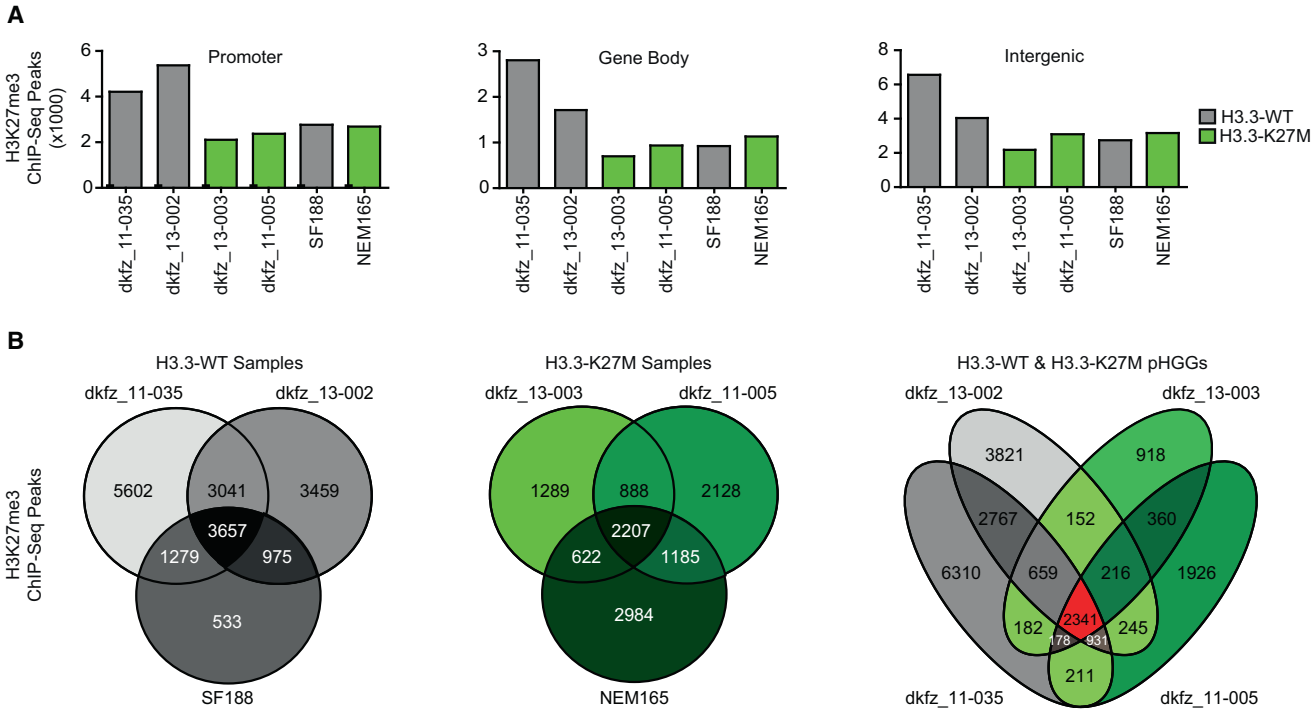

Figure 3. H3K27me3 Occupancy in Primary pHGGs and in Vitro Cultures

(A) Bar chart representing the numbers of overall H3K27me3 ChIP-Seq peaks identified in different genomic regions in four pHGGs and the two patient-derived glioblastoma cell lines, SF188 and NEM165.

(B) Venn diagrams illustrating overlapping H3K27me3 ChIP-Seq peaks in H3.3-WT and/or K27M mutant samples.

upregulated genes in K27M mutant pHGGs were found to hold decreased levels of H3K27me3 compared with H3.3-WT tumors (Figure 4B). Elevated gene expression and decreased H3K27me3 occupancy were found for several genes that are known to be involved in gliomagenesis, such as the platelet-derived growth factor receptor-α (*PDGFRA*) gene (Figure 4B; Table S2) (Verhaak et al., 2010; Zarghooni et al., 2010).

In addition to overall reduction of H3K27me3, we also identified several genes/loci with increased levels of H3K27me3 and concomitant reduction of gene expression specifically in K27M mutant pHGGs (Figures 4A and 4B; Table S2). One example showing reduced expression and a gain of H3K27me3 occupancy in its promoter in K27M mutant pHGGs was the MHC class I polypeptide-related sequence A (*MICA*) gene (Figure 4B). Downregulation of this gene has been suggested as a potential mechanism of immune evasion in malignant gliomas (Eisele et al., 2006). By comparing ChIP-Seq data of a K27M mutant DIPG cell line and NSCs, a recent study also reported on the K27M-specific gain of H3K27me3 at specific genes (Chan et al., 2013). In line with this study, the long isoform of *CDK6* was also found to hold elevated levels of H3K27me3 in both K27M mutant primary pHGGs (Figure S2D).

In keeping with the above findings, among the differentially expressed genes we found a significant ($p < 0.01$, Fisher's exact test) enrichment of genes known to be targeted by H3K27me3 (PRC2 target genes; Bernstein et al., 2006; Lee et al., 2006). Therefore, we subsequently visualized H3K27me3 occupancy around the TSSs of PRC2 target genes (n = 606; Figure 4C). Based on H3K27me3 occupancy, PRC2 target genes were divided into two groups. As expected, the large majority of these genes (n = 461) had lower H3K27me3 levels in K27M mutant pHGGs compared with H3.3-WT tumors (H3K27me3 LOSS in K27M). In line with this, average expression of these genes was significantly higher in K27M mutant pHGGs (n = 12) than in H3.3-WT samples (n = 10; Figure 4C). In contrast, PRC2 target genes holding increased levels of H3K27me3 in K27M mutant tumors (n = 145; H3K27me3 GAIN in K27M) showed reduced average expression in K27M mutant pHGGs (Figure 4C).

Alterations of H3K27me3 and DNA Methylation Establish the K27M-Specific Transcriptional Program

Numerous studies have shown a dynamic interaction between H3K27me3 and DNA methylation (Cedar and Bergman, 2009).

(E) In vitro histone H3K27 methyltransferase enzymatic assay using total chromatin lysate or immunoprecipitated HA-tagged H3.3 complexes (WT or K27M) from SF188, HEK293T, or HeLa-S3 cells (***$p < 0.001$, **$p < 0.01$, *$p < 0.05$).

(F) IC_{50} measurement of K27M peptide (AA16–46) and the EZH2 inhibitor GSK343. Assay was performed in duplicates.

(G) In vitro JMJD3/UTX histone demethylase activity assay with the same samples from HEK293T cells used in (D) (*$p < 0.05$; n.s., not significant). Error bars represent standard deviation. See also Figure S1 and Table S1.

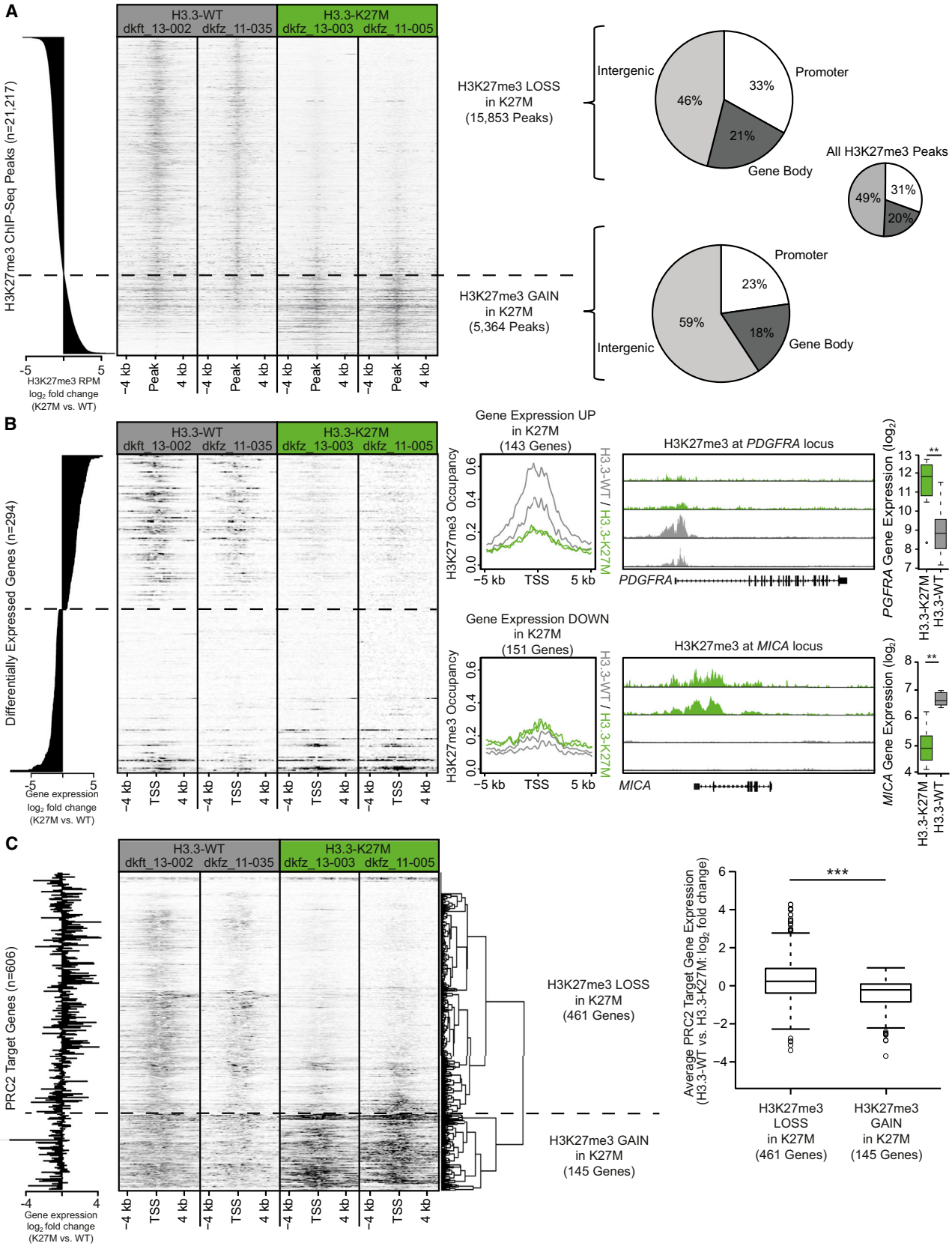

(legend on next page)

Previous work from us and others demonstrated that both of these epigenetic modifications are specifically altered in K27M mutant pHGGs (Lewis et al., 2013; Sturm et al., 2012; Venneti et al., 2013). To study DNA methylation in more detail and to find a potential cross-talk between H3K27me3 and DNA methylation in pHGGs, we subjected 13 primary tumors (six H3.3-WT and seven K27M) to whole-genome bisulfite sequencing (WGBS; see Table S4 for an overview of the WGBS statistics). Globally, K27M mutant tumors have a DNA methylation profile substantially different from that of H3.3-WT pHGGs (Figures 5A and S3A). As indicated in our previous study using DNA methylation arrays (Sturm et al., 2012), WGBS data confirmed an overall reduction in global DNA methylation levels in K27M mutant tumors compared with H3.3-WT pHGGs (Figure 5B). In line with this, we identified a substantially higher number of hypomethylated rather than hypermethylated differentially methylated regions (DMRs) in our data set when comparing K27M mutant tumors versus H3.3-WT pHGGs (Figure 5C).

Next, we analyzed overall DNA methylation patterns in genomic regions flanking the TSSs (± 5 kb) of differentially expressed genes (n = 294). As shown in Figure 5D, we found DNA hypomethylation to be specifically pronounced at genomic regions directly downstream of the TSSs of transcriptionally upregulated genes such as eyes absent homolog 1 (*EYA1*; Figure 5D; Auvergne et al., 2013). In contrast, DNA hypermethylation was found to be centered around the TSSs of transcriptionally downregulated genes such as PDZ and LIM domain 4 (*PDLIM4*; Figure 5D; de Tayrac et al., 2011). While hypomethylated DMRs were found at 54 out of 143 (38%) of transcriptionally upregulated genes, hypermethylated DMRs were identified at only 15% (22 out of 151) of downregulated genes (Table S2). However, DNA hypomethylation as well as hypermethylation were significantly associated with transcriptional activation and repression, respectively ($p < 0.01$; Fisher's exact test).

Subsequently, we aimed to find out whether regions with loss or gain of H3K27me3 were specifically associated with alterations in DNA methylation. In doing so, average DNA methylation at genomic regions flanking H3K27me3 peaks as identified by ChIP-Seq did not show significant changes (Figure S3B). However, H3K27me3 occupancy at hypomethylated gene promoters in K27M mutant pHGGs was found to be substantially lower compared with hypermethylated promoters in these tumors (Figure 5E). Although these results do not support a global link between H3K27me3 and DNA methylation, we identified a substantial number of transcriptionally activated genes such as protocadherin-7 (*PCDH7*) showing loss of H3K27me3 together with DNA hypomethylation (Figure 5E). The PRC2 target gene *PCDH7* has been shown to promote metastasis in breast cancer and is known to be targeted by DNA methylation (Beukers et al., 2013; Li et al., 2013). In total, 30% (43 out of 143) of all upregulated genes in K27M mutant pHGGs were found to hold decreased H3K27me3 levels together with DNA hypomethylation at the promoter. In contrast, only 7% (10 out of 143) of upregulated genes show DNA hypomethylation but no alteration in H3K27me3. Taken together, whereas the majority of downregulated genes in K27M mutant pHGGs (96 out of 151 genes, 64%) showed no difference in H3K27me3 or DNA methylation, the increased expression of 74% (106 out of 143) of upregulated genes might be explained by at least one of these two epigenetic mechanisms, suggesting that increased expression subsequent to a loss of gene silencing is the principle mode of direct epigenetic dysregulation in these tumors.

DISCUSSION

Deregulated H3K27me3 levels have been demonstrated in a variety of human cancers. For most of these entities, H3K27me3 levels are altered due to genetic hits within the machinery responsible for H3K27me3 turnover (Martinez-Garcia and Licht, 2010). Several findings, such as activating mutations of EZH2 (e.g., Y641) in lymphomas or overexpression of *EZH2* in numerous tumor entities, point toward an oncogenic role of *EZH2* and H3K27me3. However, a different set of mutations leading to loss of EZH2 methyltransferase activity and reduced H3K27 trimethylation indicate a dual role of *EZH2* and this histone mark in tumorigenesis, depending on context (Greer and Shi, 2012). Accordingly, reduced H3K27me3 levels are associated with unfavorable prognosis in breast, ovarian, and pancreatic cancers (Greer and Shi, 2012; Wei et al., 2008). Recently, pHGGs harboring the K27M mutation of histone H3.3 were reported to have strongly reduced H3K27me3 levels as a consequence of a dominant-negative effect of the K27M mutant H3.3 protein (Chan et al., 2013; Lewis et al., 2013; Venneti et al., 2013). Interestingly, K27M mutant pHGGs also show a trend toward inferior overall survival compared with their nonmutated counterpart (Khuong-Quang et al., 2012; Sturm et al., 2012). In this study, we demonstrate that immunohistochemical staining of H3K27me3 is a valuable tool to identify K27M mutant pHGGs with an overall accuracy of 98% using a large cohort of 104 pHGGs. This stratification may help to inform future clinical trial design and/or to identify patients who may respond to specific targeted therapy. The identification of 3% of pHGGs without

Figure 4. Alterations in H3K27me3 Occupancy in K27M Mutant pHGGs Are Directly Associated with Differential Gene Expression

(A) Heatmap illustrating H3K27me3 occupancy at 21,217 ChIP-Seq peaks identified in pHGGs. Peaks are sorted according to H3K27me3 occupancy (RPM $\log_2$ fold change: K27M versus H3.3-WT). Pie charts illustrate genomic location of ChIP-Seq peaks.

(B) Heatmap and intensity plots illustrate H3K27me3 occupancy in the genomic region flanking the TSS of differentially expressed genes (n = 294). Gene expression values ($\log_2$ fold change) are given for every differentially expressed gene. H3K27me3 occupancy in the genomic region of *PDGFRA* (chr4: 55,074,548–55,175,548) and *MICA* (chr6: 31,353,339–31,403,976) as well as corresponding gene expression in 12 K27M mutant pHGGs and 10 H3.3-WT tumors are shown as box plots (**$p < 0.01$). Box plots represent the interquartile range (IQR), with the median represented by a solid line. Bars extend to the maximum/minimum (up to 1.5 IQR). Outliers (>1.5 IQR) are plotted as circles. See also Figure S2 and Tables S2 and S3.

(C) Heatmap displaying H3K27me3 occupancy in the genomic region flanking the TSS of known PRC2 target genes (n = 606). Group separation (H3K27me3 LOSS in K27M or K27me3 GAIN in K27M) indicated by the dendrogram was based on H3K27me3 occupancy. Gene expression values ($\log_2$ fold change) determined in a cohort of 12 K27M mutant and 10 H3.3-WT pHGGs are given for each PRC2 target gene. Average gene expression ($\log_2$ fold change) of PRC2 target genes of the respective group is shown as a box plot (***$p < 0.001$). Box plots represent the IQR, with the median represented by a solid line. Bars extend to the maximum/minimum (up to 1.5 IQR). Outliers (>1.5 IQR) are plotted as circles. See also Figure S2 and Tables S2 and S3.

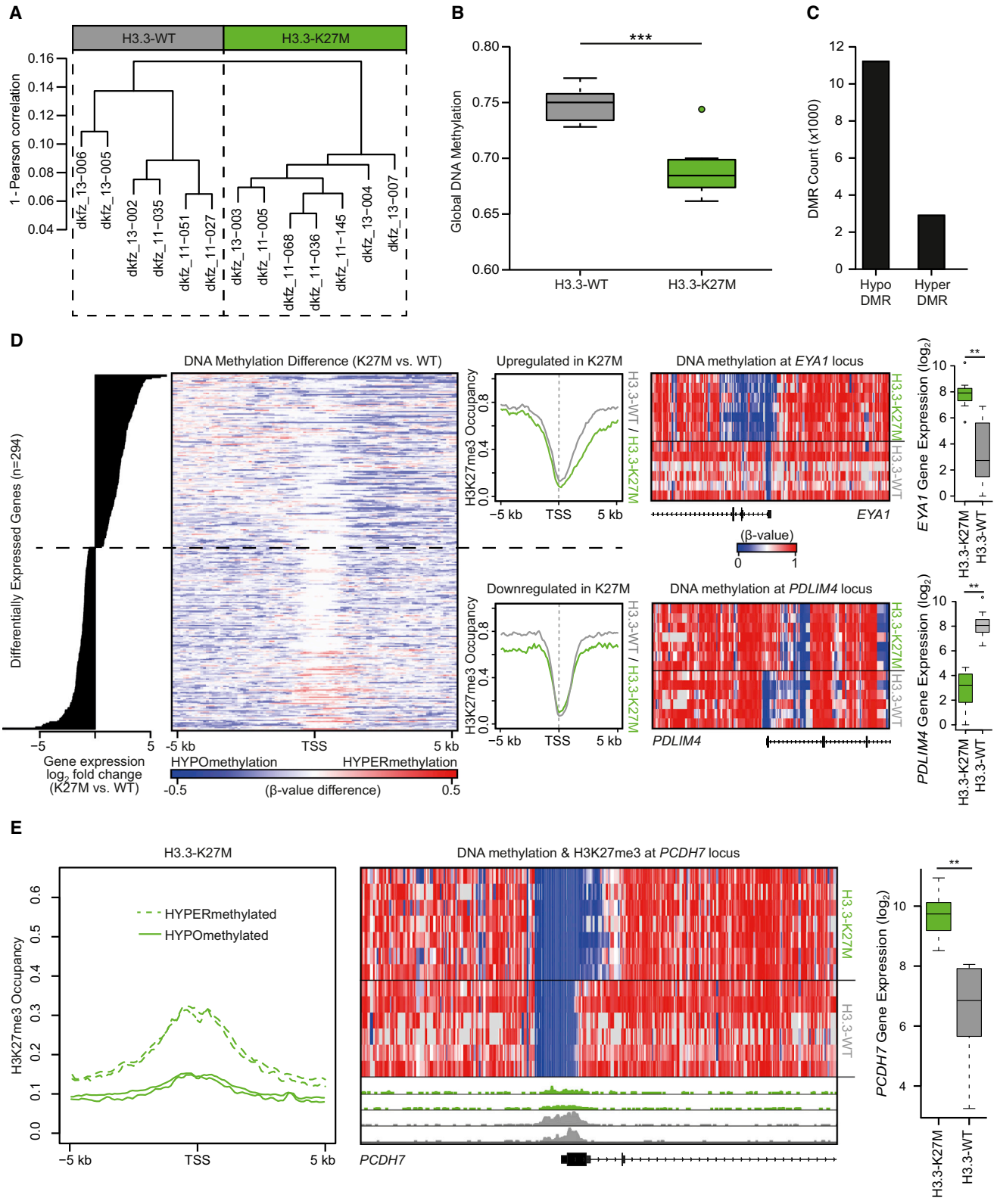

Figure 5. Global DNA Hypomethylation Contributes to Differential Gene Expressions in Concert with Loss of H3K27me3

(A) Cluster analysis of WGBS data in six H3.3-WT pHGGs and seven K27M mutant tumors.

(B) Box plot illustrating global DNA methylation levels in 13 pHGGs analyzed by WGBS (***$p < 0.001$). Box plots represent the IQR with the median represented by a solid line. Bars extend to the maximum/minimum (up to 1.5 IQR). Outliers (>1.5 IQR) are plotted as circles. See also Figure S3 and Table S4.

(legend continued on next page)

H3.3/H3.1 mutation showing similar reduced H3K27me3 levels suggests the existence of other (epi)genetic alterations affecting H3K27me3 establishment or maintenance.

Although there are conflicting data, several lines of evidence point to PRC2-mediated establishment of H3K27me3 and DNA methylation acting in parallel to modulate gene expression (Gal-Yam et al., 2008; Schlesinger et al., 2007; Viré et al., 2006; Widschwendter et al., 2007). In this study, we describe concerted alterations in H3K27me3 occupancy and DNA methylation in K27M mutant pHGGs. Both of these epigenetic mechanisms, involved in regulation of gene expression, are found to be specifically impaired in pHGGs harboring the K27M mutation of H3.3. Whereas the main focus of our study deals with the K27M-induced reduction of the repressive histone mark H3K27me3, our data also provide evidence that K27M mutant pHGGs are characterized by global DNA hypomethylation, a feature which has recently been described as being even more strongly prevalent in G34R mutant pHGGs (Sturm et al., 2012). As expected, reduced H3K27me3 and DNA hypomethylation were both found to be significantly associated with activated gene expression. Strikingly, reduced H3K27me3 alone or in combination with DNA hypomethylation was found at 74% of all transcriptionally upregulated genes in K27M mutant tumors, indicating that these are the two main mechanisms conferring the highly characteristic gene expression program.

Loss of PRC2 activity (e.g., due to depletion of EZH2 or EED) has been shown to induce changes in DNA methylation, including DNA hypomethylation (Reddington et al., 2013; Wu et al., 2008). In line with this, overexpression of K27R mutant canonical H3 was reported to lead to a significant reduction of global DNA methylation levels in human ovarian cancer cells (Abbosh et al., 2006). The high percentage (45%) of transcriptionally upregulated genes with reduced H3K27me3 levels in K27M mutant pHGGs that also showed a loss of DNA methylation suggests that K27M-induced reduction of H3K27me3 might indeed prime for DNA hypomethylation.

In addition, we aimed to find out whether K27M-induced reduction of H3K27me3 primes for DNA hypomethylation by using modified isogenic cell lines. Although these cells show a strong reduction of H3K27me3 after lentiviral overexpression of K27M mutant H3.3, we did not detect any consistent alteration in gene expression or DNA methylation in these cell lines (data not shown). In line with this, our study revealed substantial differences in H3K27me3 occupancy between primary tumor samples and pHGG cell lines. Therefore, caution is needed when attempting to extrapolate from cell models to disease pathology of different cancer entities including pHGGs in vivo (Houshdaran et al., 2010). Although our H3K27me3 ChIP-Seq data of primary pHGGs are in line with most of the recently described K27M-induced changes found by comparing a K27M mutant cell line with neural stem cells (global H3K27me3 reduction and focal gain of H3K27me3 at some loci/genes such as *CDK6*), not all conclusions generated out of a comparison of cell lines will reflect the situation in primary tumors (e.g., there are no differences in H3K27me3 peak widths between K27M mutant and H3.3-WT pHGGs; Chan et al., 2013).

Promoter hypermethylation was reported to be a general mechanism to silence known PRC2 target genes in several human cancer entities (Avissar-Whiting et al., 2011; Bennett et al., 2009; Schlesinger et al., 2007; Widschwendter et al., 2007). Interestingly, gain of H3K27me3 at the TSSs of several genes in K27M mutant pHGGs was not associated with DNA hypermethylation. This is consistent with other studies reporting on PRC2-mediated gene silencing independent of DNA hypermethylation (Kondo et al., 2008). However, the identification of specific loci with gain of H3K27me3 in the context of overall reduction of this epigenetic mark (in K27M mutant tumors) raises interesting questions about the molecular mechanisms behind PRC2 targeting, which is still a field of intense research (Simon and Kingston, 2013). A recently described model, which is based on the fact that DNA methylation attenuates PRC2 binding, might explain increased H3K27me3 levels at specific loci in K27M mutant pHGGs (Reddington et al., 2013). Global DNA hypomethylation may allow for increased binding of PRC2 and establishment of H3K27me3 at genomic sites that are normally protected by the DNA methylation mark. As a consequence, this may also enhance the reduction of H3K27me3 at normal PRC2 targets due to dilution of PRC2 molecules.

In conclusion, our study provides intriguing evidence that reduced H3K27me3 and/or DNA hypomethylation are the major driving forces of activated gene expression in K27M mutant pHGGs. Although our data suggest a potential link between K27M-induced loss of PRC2 repression and DNA hypomethylation, further work will be required to elucidate how these changes are targeted to specific genomic loci.

EXPERIMENTAL PROCEDURES

Patient and Tumor Samples

All primary tumor samples used in this study were collected at the German Cancer Research Center (DKFZ) and the Burdenko Neurosurgical Institute in accordance with the respective research ethics boards. Informed consent was obtained from all patients included in this study. An ethical vote was obtained from the ethics committee of the Medical Faculty of Heidelberg. The majority of primary tumor samples for gene expression analysis were part of a previously described study cohort (n = 17; Sturm et al., 2012). Five

(C) Overall number of DMRs in 13 pHGGs detected by WGBS.

(D) Heatmap illustrating averaged difference in DNA methylation detected by WGBS in genomic regions flanking the TSS of 294 differentially expressed genes. In addition, averaged DNA methylation levels in H3.3-WT (gray) and K27M mutant pHGGs (green) are given as intensity plots for transcriptionally upregulated and downregulated genes, respectively. DNA methylation the genomic regions flanking the TSS of *EYA1* (chr8: 72,249,222–72,300,222) and *PDLIM4* (chr5: 131,583,226–131,604,226) are shown as examples together with gene expression (log_2) in 12 K27M mutant pHGGs and 10 H3.3-WT tumors illustrated by box blots (**$p < 0.01$). Box plots represent the IQR with the median represented by a solid line. Bars extend to the maximum/minimum (up to 1.5 IQR). Outliers (>1.5 IQR) are plotted as circles.

(E) Intensity plot illustrating H3K27me3 occupancy around the TSS of genes found to be hypo- or hypermethylated in K27M mutant pHGGs. DNA methylation as well as H3K27me3 occupancy at the genomic region of *PCDH7* (chr4: 30,687,866–30,768,866) is shown as an example together with corresponding gene expression data (log_2) in 12 K27M mutant pHGGs and 10 H3.3-WT tumors illustrated by box blots (**$p < 0.01$). Box plots represent the IQR with the median represented by a solid line. Bars extend to the maximum/minimum (up to 1.5 IQR). Outliers (>1.5 IQR) are plotted as circles. See also Figure S3 and Table S4.

additional tumor samples were analyzed on the Affymetrix GeneChip Human GenomeU133 Plus 2.0 Array. A list of all used primary tumor samples and their use in the study of Sturm et al. (2012) is provided in Supplemental Experimental Procedures.

Immunohistochemistry

Tumor cores or whole tumor sections of 104 pHGGs with known *H3F3A* mutation status were stained for H3K27me3 by using the following antibody: H3K27me3 (Millipore 07-449).

Western Blot Analysis

The Histone Purification Mini Kit (Active Motif) was used to isolate and purify histone proteins followed by electrophoretic separation and transfer to a polyvinylidene fluoride membrane. Antibodies against the following antigens were applied: H3K27me3 (Millipore 07-449), H3K27me3 (Abcam ab6002), H3K27me2 (Abcam ab24684), H3K27me1 (Abcam 07-448), HA-tag (Abcam ab9110), histone H4 (Abcam ab10158), H3 (Abcam ab1791), SUZ12 (Active Motif 39357), and EZH2 (Active Motif 39933).

Generation of H3.3-Overexpressing Cell Lines

SF188 glioblastoma cells (University of California, San Francisco), HEK293T cells (ATCC), or HeLa-S3 cells (ATCC) were lentivirally transduced (multiplicity of infection of 5) using the open reading frame of H3.3 cloned into pLVX-Puro (Clontech) or pCDH1-CMV-MCS-EF1-copGFP backbone (System Bio). Both H3.3 mutants were generated by using the QuikChange II Site-Directed Mutagenesis Kit (Agilent).

Cell Culture

HEK293T, HeLa-S3, SF188, MGBM1, and KNS42 cells were cultured in high glucose Dulbecco's modified Eagle's medium (Life Technologies) supplemented with 10% fetal calf serum (GIBCO) at 37°C and 5% CO_2. NEM157 and NEM165 primary pHGG cells were cultured in AmniomaxC100 + 10% AmniomaxC100 supplement (GIBCO). Upon reaching a confluency of 80%, cells were trypsinized and used for protein extraction.

Coimmunoprecipitation

To compare the binding of PRC2 complex components with H3.3-WT or K27M mutant protein, mono-nucleosome IP was performed with EZview Red Anti-HA Affinity Gel or anti-EZH2 antibody (Active Motif 39901) using HA-tagged H3.3 (WT or K27M)-transduced HEK293T, HeLa-S3, or SF188 cells. The precipitates were analyzed by western blot using antibodies against EZH2, SUZ12, and HA, as indicated.

Chromatin Lysate Preparation and Mono-Nucleosome IP

Cells were harvested by centrifugation and washed in PBS before cell lysis. Cell nuclei were pelleted and lysed to collect insoluble chromatin followed by MNase digestion. For mono-nucleosome IP, EZview Red Anti-HA Affinity Gel (Sigma E6779) was added into the chromatin lysate. After incubation at 4°C overnight, samples were analyzed by western blot using the indicated antibodies.

In Vitro Histone Methyltransferase/Demethylase Assay

In vitro HMT assays were performed using the EpiQuik Histone Methyltransferase Activity/Inhibition Assay Kit (H3K27; Epigentek; P-3005-96). In vitro histone demethylase assays were performed using the Epigenase JMJD3/UTX Demethylase Activity/Inhibition Assay Kit (Fluorometric; Epigentek; P-3085-48). The assays were performed using either chromatin lysate or anti-HA beads after mono-nucleosome IP, as per the manufacturer's instructions.

H3K27me3 ChIP-Seq Sequencing and Data Processing

H3K27me3 ChIP-Seq of primary pHGG samples and cell lines has been performed at Active Motif according to proprietary methods. Libraries were sequenced on the Illumina HiSeq 2000 platform. To make the number of detected peaks comparable between samples, we first applied Picard DownsampleSam to equalize the number properly paired reads per sample.

Whole-Genome Bisulfite Sequencing and Data Processing

Strand-specific MethylC-seq libraries were prepared using a previously described approach with modifications (Lister et al., 2011). Adaptor-ligated DNA fragments with insert lengths of 200–250 bp were isolated and bisulfite converted using the EZ DNA Methylation kit (Zymo Research). After PCR amplification, libraries were sequenced on the Illumina HiSeq 2000 platform. An overview of generated WGBS data is provided in Table S4. Differentially methylated regions (DMRs) were identified using the bsseq Bioconductor package, version 0.6.2 (Hansen et al., 2012).

Integrative Genomic Analysis

Downstream analyses were performed in R, version 2.15.2 (R Development Core Team, 2012). Genes were termed differentially expressed between K27M-mutatnt and H3.3-WT tumors when displaying an adjusted p value < 0.01 (Student's t test, Benjamini-Hochberg correction for multiple testing). Overlapping H3K27me3 ChIP-Seq peaks in the four clinical samples were merged and mean reads per million (RPM) values for all samples were extracted from the whole-genome coverage tracks. Merged peaks within ±3 kb of the TSS were associated with annotated RefSeq genes. For heatmap representations of H3K27me3 occupancy surrounding merged peaks or TSSs, RPM values were extracted from the whole-genome coverage tracks with a window size of 100, effectively separating the depicted 10-kb region into 100 equally sized bins. Heatmaps were vertically ordered by mean RPMs in the combined peak region. Hierarchical clustering in Figure 4C was performed using Euclidean distance and complete linkage.

All DMRs associated with a RefSeq gene annotation (within ±3 kb of the TSS [hyper DMRs] and −3/+20 kb of the TSS [hypo DMRs]) were combined per gene, independently for hypo- and hypermethylated DMRs. Heatmap representations of DNA methylation were generated by separating the depicted 10-kb region into 100 equally sized bins.

ACCESSION NUMBERS

Microarray expression data of 22 tumor samples are available in National Center for Biotechnology Information's Gene Expression Omnibus (GEO; http://www.ncbi.nlm.nih.gov/geo) through GEO Series accession numbers GSE36245, GSE34824, and GSE49822. H3K27me3 ChIP-Seq and WGBS data are available through European Genome-phenome Archive accession number EGAS00001000578.

SUPPLEMENTAL INFORMATION

Supplemental Information includes Supplemental Experimental Procedures, three figures, and four tables and can be found with this article online at http://dx.doi.org/10.1016/j.ccr.2013.10.006.

ACKNOWLEDGMENTS

We would like to thank Laura Sieber and Andrea Wittmann from the Division of Pediatric Neurooncology at the DKFZ for excellent technical support. The project was supported by grants from the German Cancer Aid (109252 and 108456) and the Federal Ministry of Education and Research (to P.L. and S.M.P.; International Cancer Genome Consortium PedBrain, NGFNPlus #01GS0883); St. Baldrick's Foundation (to Y.J.C), National Institutes of Health K08NS070926 (to M.M.); and National Health Service funding to the National Institute for Health Research Biomedical Research Centre (to C.J.). This work was also supported by funds from the Center for Children's Brain Tumors at Stanford (to Y.J.C. and M.M.), a Beirne Faculty Scholar endowment at Stanford (to Y.J.C. and M.M.), Alex's Lemonade Stand Foundation (to M.M.), the McKenna Claire Foundation (to M.M.), The Cure Starts Now (to M.M.), the Lyla Nsouli Foundation (to M.M.), the Connor Johnson Memorial Fund (to M.M.), the Dylan Jewett Memorial Fund (to M.M.), the Dylan Frick Memorial Fund (to M.M.), the Abigail Jensen Memorial Fund (to M.M.), the Zoey Ganesh Memorial Fund (to M.M.), and "L'Etoile de Martin" (to N.T., D.C., and J.G.). The authors would like to thank Joanna Wysocka for helpful discussions.

Received: March 29, 2013
Revised: August 9, 2013
Accepted: October 4, 2013
Published: October 31, 2013

REFERENCES

Abbosh, P.H., Montgomery, J.S., Starkey, J.A., Novotny, M., Zuhowski, E.G., Egorin, M.J., Moseman, A.P., Golas, A., Brannon, K.M., Balch, C., et al. (2006). Dominant-negative histone H3 lysine 27 mutant derepresses silenced tumor suppressor genes and reverses the drug-resistant phenotype in cancer cells. Cancer Res. *66*, 5582–5591.

Auvergne, R.M., Sim, F.J., Wang, S., Chandler-Militello, D., Burch, J., Al Fanek, Y., Davis, D., Benraiss, A., Walter, K., Achanta, P., et al. (2013). Transcriptional differences between normal and glioma-derived glial progenitor cells identify a core set of dysregulated genes. Cell Rep. *3*, 2127–2141.

Avissar-Whiting, M., Koestler, D.C., Houseman, E.A., Christensen, B.C., Kelsey, K.T., and Marsit, C.J. (2011). Polycomb group genes are targets of aberrant DNA methylation in renal cell carcinoma. Epigenetics *6*, 703–709.

Bennett, L.B., Schnabel, J.L., Kelchen, J.M., Taylor, K.H., Guo, J., Arthur, G.L., Papageorgio, C.N., Shi, H., and Caldwell, C.W. (2009). DNA hypermethylation accompanied by transcriptional repression in follicular lymphoma. Genes Chromosomes Cancer *48*, 828–841.

Bernstein, B.E., Mikkelsen, T.S., Xie, X., Kamal, M., Huebert, D.J., Cuff, J., Fry, B., Meissner, A., Wernig, M., Plath, K., et al. (2006). A bivalent chromatin structure marks key developmental genes in embryonic stem cells. Cell *125*, 315–326.

Beukers, W., Hercegovac, A., Vermeij, M., Kandimalla, R., Blok, A.C., van der Aa, M.M., Zwarthoff, E.C., and Zuiverloon, T.C. (2013). Hypermethylation of the polycomb group target gene PCDH7 in bladder tumors from patients of all ages. J. Urol. *190*, 311–316.

Cedar, H., and Bergman, Y. (2009). Linking DNA methylation and histone modification: patterns and paradigms. Nat. Rev. Genet. *10*, 295–304.

Chan, K.M., Fang, D., Gan, H., Hashizume, R., Yu, C., Schroeder, M., Gupta, N., Mueller, S., James, C.D., Jenkins, R., et al. (2013). The histone H3.3K27M mutation in pediatric glioma reprograms H3K27 methylation and gene expression. Genes Dev. *27*, 985–990.

de Tayrac, M., Aubry, M., Saikali, S., Etcheverry, A., Surbled, C., Guenot, F., Galibert, M.D., Hamlat, A., Lesimple, T., Quillien, V., et al. (2011). A 4-gene signature associated with clinical outcome in high-grade gliomas. Clin. Cancer Res. *17*, 317–327.

Eisele, G., Wischhusen, J., Mittelbronn, M., Meyermann, R., Waldhauer, I., Steinle, A., Weller, M., and Friese, M.A. (2006). TGF-β and metalloproteinases differentially suppress NKG2D ligand surface expression on malignant glioma cells. Brain *129*, 2416–2425.

Fontebasso, A.M., Schwartzentruber, J., Khuong-Quang, D.A., Liu, X.Y., Sturm, D., Korshunov, A., Jones, D.T., Witt, H., Kool, M., Albrecht, S., et al. (2013). Mutations in SETD2 and genes affecting histone H3K36 methylation target hemispheric high-grade gliomas. Acta Neuropathol. *125*, 659–669.

Gal-Yam, E.N., Egger, G., Iniguez, L., Holster, H., Einarsson, S., Zhang, X., Lin, J.C., Liang, G., Jones, P.A., and Tanay, A. (2008). Frequent switching of Polycomb repressive marks and DNA hypermethylation in the PC3 prostate cancer cell line. Proc. Natl. Acad. Sci. USA *105*, 12979–12984.

Greer, E.L., and Shi, Y. (2012). Histone methylation: a dynamic mark in health, disease and inheritance. Nat. Rev. Genet. *13*, 343–357.

Hansen, K.D., Langmead, B., and Irizarry, R.A. (2012). BSmooth: from whole genome bisulfite sequencing reads to differentially methylated regions. Genome Biol. *13*, R83.

Houshdaran, S., Hawley, S., Palmer, C., Campan, M., Olsen, M.N., Ventura, A.P., Knudsen, B.S., Drescher, C.W., Urban, N.D., Brown, P.O., and Laird, P.W. (2010). DNA methylation profiles of ovarian epithelial carcinoma tumors and cell lines. PLoS ONE *5*, e9359.

Khuong-Quang, D.A., Buczkowicz, P., Rakopoulos, P., Liu, X.Y., Fontebasso, A.M., Bouffet, E., Bartels, U., Albrecht, S., Schwartzentruber, J., Letourneau, L., et al. (2012). K27M mutation in histone H3.3 defines clinically and biologically distinct subgroups of pediatric diffuse intrinsic pontine gliomas. Acta Neuropathol. *124*, 439–447.

Kondo, Y., Shen, L., Cheng, A.S., Ahmed, S., Boumber, Y., Charo, C., Yamochi, T., Urano, T., Furukawa, K., Kwabi-Addo, B., et al. (2008). Gene silencing in cancer by histone H3 lysine 27 trimethylation independent of promoter DNA methylation. Nat. Genet. *40*, 741–750.

Lee, T.I., Jenner, R.G., Boyer, L.A., Guenther, M.G., Levine, S.S., Kumar, R.M., Chevalier, B., Johnstone, S.E., Cole, M.F., Isono, K., et al. (2006). Control of developmental regulators by Polycomb in human embryonic stem cells. Cell *125*, 301–313.

Lewis, P.W., Müller, M.M., Koletsky, M.S., Cordero, F., Lin, S., Banaszynski, L.A., Garcia, B.A., Muir, T.W., Becher, O.J., and Allis, C.D. (2013). Inhibition of PRC2 activity by a gain-of-function H3 mutation found in pediatric glioblastoma. Science *340*, 857–861.

Li, A.M., Tian, A.X., Zhang, R.X., Ge, J., Sun, X., and Cao, X.C. (2013). Protocadherin-7 induces bone metastasis of breast cancer. Biochem. Biophys. Res. Commun. *436*, 486–490.

Lister, R., Pelizzola, M., Kida, Y.S., Hawkins, R.D., Nery, J.R., Hon, G., Antosiewicz-Bourget, J., O'Malley, R., Castanon, R., Klugman, S., et al. (2011). Hotspots of aberrant epigenomic reprogramming in human induced pluripotent stem cells. Nature *471*, 68–73.

Louis, D.N., Ohgaki, H., Wiestler, O.D., Cavenee, W.K., Burger, P.C., Jouvet, A., Scheithauer, B.W., and Kleihues, P. (2007). The 2007 WHO classification of tumours of the central nervous system. Acta Neuropathol. *114*, 97–109.

Margueron, R., and Reinberg, D. (2011). The Polycomb complex PRC2 and its mark in life. Nature *469*, 343–349.

Martinez-Garcia, E., and Licht, J.D. (2010). Deregulation of H3K27 methylation in cancer. Nat. Genet. *42*, 100–101.

R Development Core Team (2012). R: A language and environment for statistical computing. R Foundation for Statistical Computing, Vienna. ISBN 3-900051-07-0, http://www.R-project.org.

Reddington, J.P., Perricone, S.M., Nestor, C.E., Reichmann, J., Youngson, N.A., Suzuki, M., Reinhardt, D., Dunican, D.S., Prendergast, J.G., Mjoseng, H., et al. (2013). Redistribution of H3K27me3 upon DNA hypomethylation results in de-repression of Polycomb target genes. Genome Biol. *14*, R25.

Schlesinger, Y., Straussman, R., Keshet, I., Farkash, S., Hecht, M., Zimmerman, J., Eden, E., Yakhini, Z., Ben-Shushan, E., Reubinoff, B.E., et al. (2007). Polycomb-mediated methylation on Lys27 of histone H3 pre-marks genes for de novo methylation in cancer. Nat. Genet. *39*, 232–236.

Schwartzentruber, J., Korshunov, A., Liu, X.Y., Jones, D.T., Pfaff, E., Jacob, K., Sturm, D., Fontebasso, A.M., Quang, D.A., Tönjes, M., et al. (2012). Driver mutations in histone H3.3 and chromatin remodelling genes in paediatric glioblastoma. Nature *482*, 226–231.

Simon, J.A., and Kingston, R.E. (2013). Occupying chromatin: Polycomb mechanisms for getting to genomic targets, stopping transcriptional traffic, and staying put. Mol. Cell *49*, 808–824.

Sturm, D., Witt, H., Hovestadt, V., Khuong-Quang, D.A., Jones, D.T., Konermann, C., Pfaff, E., Tönjes, M., Sill, M., Bender, S., et al. (2012). Hotspot mutations in H3F3A and IDH1 define distinct epigenetic and biological subgroups of glioblastoma. Cancer Cell *22*, 425–437.

Turcan, S., Rohle, D., Goenka, A., Walsh, L.A., Fang, F., Yilmaz, E., Campos, C., Fabius, A.W., Lu, C., Ward, P.S., et al. (2012). IDH1 mutation is sufficient to establish the glioma hypermethylator phenotype. Nature *483*, 479–483.

Venneti, S., Garimella, M.T., Sullivan, L.M., Martinez, D., Huse, J.T., Heguy, A., Santi, M., Thompson, C.B., and Judkins, A.R. (2013). Evaluation of histone 3 lysine 27 trimethylation (H3K27me3) and enhancer of zest 2 (EZH2) in pediatric glial and glioneuronal tumors shows decreased H3K27me3 in H3F3A K27M mutant glioblastomas. Brain Pathol. *23*, 558–564.

Verhaak, R.G., Hoadley, K.A., Purdom, E., Wang, V., Qi, Y., Wilkerson, M.D., Miller, C.R., Ding, L., Golub, T., Mesirov, J.P., et al.; Cancer Genome Atlas Research Network. (2010). Integrated genomic analysis identifies clinically

relevant subtypes of glioblastoma characterized by abnormalities in PDGFRA, IDH1, EGFR, and NF1. Cancer Cell *17*, 98–110.

Verma, S.K., Tian, X., LaFrance, L.V., Duquenne, C., Suarez, D.P., Newlander, K.A., Romeril, S.P., Burgess, J.L., Grant, S.W., Brackley, J.A., et al. (2012). Identification of potent, selective, cell-active inhibitors of the histone lysine methyltransferase EZH2. ACS Med. Chem. Lett. *3*, 1091–1096.

Viré, E., Brenner, C., Deplus, R., Blanchon, L., Fraga, M., Didelot, C., Morey, L., Van Eynde, A., Bernard, D., Vanderwinden, J.M., et al. (2006). The Polycomb group protein EZH2 directly controls DNA methylation. Nature *439*, 871–874.

Wei, Y., Xia, W., Zhang, Z., Liu, J., Wang, H., Adsay, N.V., Albarracin, C., Yu, D., Abbruzzese, J.L., Mills, G.B., et al. (2008). Loss of trimethylation at lysine 27 of histone H3 is a predictor of poor outcome in breast, ovarian, and pancreatic cancers. Mol. Carcinog. *47*, 701–706.

Widschwendter, M., Fiegl, H., Egle, D., Mueller-Holzner, E., Spizzo, G., Marth, C., Weisenberger, D.J., Campan, M., Young, J., Jacobs, I., and Laird, P.W. (2007). Epigenetic stem cell signature in cancer. Nat. Genet. *39*, 157–158.

Wu, X., Gong, Y., Yue, J., Qiang, B., Yuan, J., and Peng, X. (2008). Cooperation between EZH2, NSPc1-mediated histone H2A ubiquitination and Dnmt1 in HOX gene silencing. Nucleic Acids Res. *36*, 3590–3599.

Wu, G., Broniscer, A., McEachron, T.A., Lu, C., Paugh, B.S., Becksfort, J., Qu, C., Ding, L., Huether, R., Parker, M., et al.; St. Jude Children's Research Hospital–Washington University Pediatric Cancer Genome Project. (2012). Somatic histone H3 alterations in pediatric diffuse intrinsic pontine gliomas and non-brainstem glioblastomas. Nat. Genet. *44*, 251–253.

Zarghooni, M., Bartels, U., Lee, E., Buczkowicz, P., Morrison, A., Huang, A., Bouffet, E., and Hawkins, C. (2010). Whole-genome profiling of pediatric diffuse intrinsic pontine gliomas highlights platelet-derived growth factor receptor alpha and poly (ADP-ribose) polymerase as potential therapeutic targets. J. Clin. Oncol. *28*, 1337–1344.